Ecophysiological variables retrieval and early stress detection: insights from a synthetic spatial scaling exercise

Javier Pacheco-Labrador, M.Pilar Cendrero-Mateo, Shari Van Wittenberghe, Itza Hernandez-Sequeira, Gerbrand Koren, Egor Prikaziuk, Szilvia Fóti, Enrico Tomelleri, Kadmiel Maseyk, Nataša Čereković, Rosario Gonzalez-Cascon, Zbyněk Malenovský, Mar Albert-Saiz, Michal Antala, János Balogh, Henning Buddenbaum, Mohammad Hossain Dehghan-Shoar, Joseph T. Fennell, Jean-Baptiste Féret, Hamadou Balde, Miriam Machwitz, Ádám Mészáros, Guofang Miao, Miguel Morata, Paul Naethe, Zoltán Nagy, Krisztina Pintér, R. Reddy Pullanagari, Anshu Rastogi, Bastian Siegmann, Sheng Wang, Chenhui Zhang & Daniel Kopkáně

View supplementary material

Published online: 28 Oct 2024.

Submit your article to this journal

Taylor & Francis
Taylor & Francis Group

Ecophysiological variables retrieval and early stress detection: insights from a synthetic spatial scaling exercise

Javier Pacheco-Labrador [a,b], M.Pilar Cendrero-Mateo [c], Shari Van Wittenberghe [c], Itza Hernandez-Sequeira [d], Gerbrand Koren [e], Egor Prikaziuk [f], Szilvia Fóti [g,h], Enrico Tomelleri [i], Kadmiel Maseyk [j], Nataša Čereković [k], Rosario Gonzalez-Cascon [l], Zbyněk Malenovský [m], Mar Albert-Saiz [n], Michal Antala [n], János Balogh [g], Henning Buddenbaum [o], Mohammad Hossain Dehghan-Shoar[p], Joseph T. Fennell [j], Jean-Baptiste Féret [q], Hamadou Balde[r], Miriam Machwitz [s], Ádám Mészáros [g], Guofang Miao [t], Miguel Morata [c], Paul Naethe [u], Zoltán Nagy [g,h], Krisztina Pintér [g,h], R. Reddy Pullanagari [v], Anshu Rastogi [n], Bastian Siegmann [w], Sheng Wang [x,y], Chenhui Zhang [z] and Daniel Kopkáně[aa]

[a]Environmental Remote Sensing and Spectroscopy Laboratory (SpecLab), Spanish National Research Council, Madrid, Spain; [b]Max Planck Institute for Biogeochemistry, Jena, Germany; [c]Laboratory of Earth Observation, Image Processing Laboratory, University of Valencia, Paterna (Valencia), Spain; [d]Institute of New Imaging Technologies, University Jaume I, Castellón de la Plana (Castellón), Spain; [e]Copernicus Institute of Sustainable Development, Utrecht University, Utrecht, The Netherlands; [f]Faculty of Geo-Information Science and Earth Observation (ITC), University of Twente, Enschede, The Netherlands; [g]Department of Plant Physiology and Plant Ecology, Institute of Agronomy, Hungarian University of Agriculture and Life Sciences, Gödöllő, Hungary; [h]HUN-REN-MATE Agroecology Research Group, Gödöllő, Hungary; [i]Faculty of Agricultural, Environmental and Food Sciences, Free University of Bozen/Bolzano, Bozen-Bolzan, Italy; [j]School of Environment, Earth and Ecosystem Sciences, The Open University, Milton Keynes, UK; [k]University of Banja Luka, Centre for Development and Research Support, Institute of Genetic Resources, Banja Luka, Bosnia and Herzegovina; [l]INIA-CSIC, Department of Environment and Agronomy, Madrid, Spain; [m]Remote Sensing Research Group, Department of Geography, University of Bonn, Bonn, Germany; [n]Laboratory of Bioclimatology, Department of Ecology and Environmental Protection, Faculty of Environmental and Mechanical Engineering, Poznań University of Life Sciences, Poznań, Poland; [o]Environmental Remote Sensing and Geoinformatics, Trier University, Trier, Germany; [p]School of Agriculture and Environment, Massey University, Palmerston North, New Zealand; [q]TETIS, INRAE, AgroParisTech, CIRAD, CNRS, Université Montpellier, Montpellier, France; [r]Laboratoire de Météorologie Dynamique, Sorbonne Université, IPSL, CNRS/L'École polytechnique, Palaiseau Cedex, France; [s]Remote sensing and natural resources modelling, Department for Environmental Research and Innovation (ERIN), Luxembourg Institute of Science and Technology (LIST), Belvaux, Luxembourg; [t]School of Geographical Sciences, Fujian Normal University, Fuzhou City, China; [u]JB Hyperspectral Devices, Düsseldorf, Germany; [v]Australian Plant Phenomics Facility (APPF), The Plant Accelerator, School of Agriculture, Food and Wine, University of Adelaide, Urrbrae, Australia; [w]Institute of Bio- and Geosciences, IBG-2: Plant Sciences, Jülich, Germany; [x]Department of Agroecology, Aarhus University, Department of Agroecology, Aarhus, Denmark; [y]Agroecosystem Sustainability Center, University of Illinois Urbana-Champaign, Agroecosystem Sustainability Center, Institute for Sustainability, Energy, and Environment, University of Illinois Urbana-Champaign, Urbana, IL, USA; [z]Institute for Data, Systems, and Society, Massachusetts Institute of Technology, Cambridge, MA, USA; [aa]Global Change Research Institute of the Czech Academy of Sciences (CzechGlobe), Bělidla, Czech Republic

CONTACT Javier Pacheco-Labrador ✉ javier.pacheco@csic.es Environmental Remote Sensing and Spectroscopy Laboratory (SpecLab), Spanish National Research Council, Albasanz 26-28, Madrid 28037, Spain

This article has been corrected with minor changes. These changes do not impact the academic content of the article.
Supplemental data for this article can be accessed online at https://doi.org/10.1080/01431161.2024.2414435

ABSTRACT

The ability to access physiologically driven signals, such as surface temperature, photochemical reflectance index (PRI), and sun-induced chlorophyll fluorescence (SIF), through remote sensing (RS) are exciting developments for vegetation studies. Accessing this ecophysiological information requires considering processes operating at scales from the top-of-the-canopy to the photosystems, adding complexity compared to reflectance index-based approaches. To investigate the maturity and knowledge of the growing RS community in this area, COST Action CA17134 SENSECO organized a Spatial Scaling Challenge (SSC). Challenge participants were asked to retrieve four key ecophysiological variables for a field each of maize and wheat from a simulated field campaign: leaf area index (LAI), leaf chlorophyll content (C_{ab}), maximum carboxylation rate ($V_{cmax,25}$), and non-photochemical quenching (NPQ). The simulated campaign data included hyperspectral optical, thermal and SIF imagery, together with ground sampling of the four variables. Non-parametric methods that combined multiple spectral domains and field measurements were used most often, thereby indirectly performing the top-of-the-canopy to photosystem scaling. LAI and C_{ab} were reliably retrieved in most cases, whereas $V_{cmax,25}$ and NPQ were less accurately estimated and demanded information ancillary to RS imagery. The factors considered least by participants were the biophysical and physiological canopy vertical profiles, the spatial mismatch between RS sensors, the temporal mismatch between field sampling and RS acquisition, and measurement uncertainty. Furthermore, few participants developed NPQ maps into stress maps or provided a deeper analysis of their parameter retrievals. The SSC shows that, despite advances in statistical and physically based models, the vegetation RS community should improve how field and RS data are integrated and scaled in space and time. We expect this work will guide newcomers and support robust advances in this research field.

1. Introduction

Remote sensing (RS) is widely used to monitor a range of vegetation attributes across scales. Mapping plant ecophysiological traits from spectral imagery is necessary for enhancing agricultural production (Weiss, Jacob, and Duveiller 2020), forest management (Lechner, Foody, and Boyd 2020), and sustaining ecosystem services (Del Río-Mena et al. 2020). The measurement and regular monitoring of both natural and managed ecosystems across time and space play a key role in our efforts to understand drivers and variations in productivity and ecosystem–climate interactions (Rocchini and Lenoir 2021; J. Yang et al. 2013). As more frequent and intense stress events are being recorded due to climate change and environmental variations (IPCC 2023), the need for early stress detection and recommendations for resource use efficiency in agriculture and forestry (Herrmann and Berger 2021) also increases.

Light and carbon dioxide are two resources that drive vegetation (primary) productivity, which depends on the absorption and use efficiency of light energy (Haxeltine and Prentice 1996) and carbon dioxide assimilation through stomata (Gates 1968).

Characterizing the ecophysiological parameters related to photosynthesis is fundamental to understanding vegetation functions and responses to the environment. Parameters that are typically quantified from field and laboratory measurements include the fraction of photosynthetically active radiation absorbed by leaves, leaf chlorophyll a and b content (C_{ab}), the maximal rate of CO_2 carboxylation at 25°C ($V_{cmax,25}$), and photosystem II quantum yields. Light energy that is not used for CO_2 assimilation and is dissipated by xanthophyll cycle pigments is characterized by the level of non-photochemical quenching (NPQ) or the thermal dissipation of absorbed photosynthetically active radiation (PAR) (Demmig-Adams et al. 2012). As NPQ increases under energy-limiting conditions, it can be used as a stress or potential stress indicator. In addition, photosynthetic efficiency depends on temperature, and optimal functioning involves stomatal control to balance CO_2 assimilation against water loss in the process of transpirational cooling (Farquhar and Sharkey 1982; Gates 1968). Usually, determining these parameters involves intensive field measurements at the leaf scale. While these measurements offer fundamental insights into the leaf-level processes, time and other resource constraints limit the extent and frequency of acquisition and, therefore, the capability of becoming monitoring tools.

The fundamental link to the absorption and use of visible light enables some of these parameters to be inferred from top-of-canopy (TOC) RS observations and, thus, the opportunity to measure and monitor vegetation status and productivity across spatial scales from field to global and at high temporal frequency. Traditionally, these observations have relied on reflected visible and infra-red radiance and derived vegetation indices (VI) related to vegetation structure, biochemistry, and photosynthetic capacity that vary over medium time scales (Nemani et al. 2003; Running et al. 2004). Recent advances in satellite technology are providing the opportunity to collect signals more closely related to dynamic vegetation properties and ecophysiological traits (Schimel et al. 2019). These include hyperspectral Visible-Near InfraRed (VNIR) reflected radiance that enables the quantification of solar-induced chlorophyll fluorescence (SIF) and the Photochemical Reflectance Index (PRI), as well as thermal infrared data for land surface temperature (LST) mapping. These signals are influenced by biophysical properties and ecophysiological processes at both canopy and leaf levels, exhibiting variations from diurnal to seasonal scales (Farella et al. 2022). Sound physiological understanding of these signals requires solving the spatial and temporal-scale mismatches between RS and field data (Ma et al. 2020). Facing such problems requires down-scaling information from canopy to leaf and even photosystem scales (Van Wittenberghe et al. 2021) for reliable interpretation of these signals and reconciling the large temporal variation of many processes with the periodic image acquisition of RS data.

Incoming radiation reaching the leaf is absorbed, reflected, and transmitted through the leaf, and part of the absorbed fraction is emitted as fluorescence or thermal radiation, with all these processes carrying ecophysiological information. However, light is scattered and reabsorbed within the plant canopy's vertical profile before escaping back to space, making it difficult to relate leaf-level physiological processes to spectral signals measured from the TOC. The RS community has developed various methodologies for estimating structural and foliar vegetation properties (Verrelst et al. 2015). Irrespective of the approach taken, the combination of RS and field information remains challenging and requires accounting for the existing spatial and temporal mismatches and the differences in environmental and physiological conditions of the different measurements.

Furthermore, these approaches might not have matured to estimate the most sensitive physiological variables (e.g. $V_{cmax,25}$, NPQ), whose weak effects on the spectral signals present an additional challenge. The interpretation of RS information without prior knowledge of the vegetation state is rare (e.g. factorial experiments), and the capability of the RS community in this regard is largely untested (Ma et al. 2020).

Several studies have evaluated the strengths and weaknesses of the retrieval methods to estimate biophysical variables featuring low diurnal variability and strong effects on spectral information, such as Cab and leaf area index (LAI) (Verrelst et al. 2019). However, there is limited information on how these methods perform when down-scaling physiological variables with subtle contributions to spectral signals and are driven by diurnal meteorology, such as $V_{cmax,25}$ and NPQ (Damm et al. 2022). It is equally important to understand the level of uncertainty associated with these estimates (Malenovský et al. 2019). Furthermore, it is worth considering how the RS scientific community integrates a series of sequential field measurements of these dynamic ecophysiological variables with usually instantaneous RS imagery. An additional problem is the interpretation of these sources of information, as most studies are carried out in controlled experiments, where the sources and levels of stress are known beforehand (e.g. Damm et al. (2022)). However, RS interpretations are expected to provide reliable conclusions from decontextualized situations, which have rarely been systematically assessed and reported in publications.

Within the context of the COST Action CA17134 SENSECO 'Optical synergies for spatiotemporal SENsing of Scalable ECOphysiological traits' (www.senseco.eu), we set out to challenge the scientific community to retrieve relevant biophysical and physiological variables from a simulated dataset of remotely sensed reflectance factors, chlorophyll sun-induced fluorescence, and thermal imagery, as well as field measurements. Specifically, the objectives for every scientist joining this study were to:

(1) down-scale the biophysical and plant physiological variables C_{ab}, LAI, $V_{cmax,25}$, and NPQ from simulated hyperspectral and thermal imagery and
(2) evaluate the capability of RS data to diagnose and discriminate between different plant ecophysiological states and translate the retrieved variables into low or high vegetation efficiency or stress.

To assess the quality of the results, we asked the participants of this study to provide the uncertainty for each of the required parameters and stress maps. The overarching goal of the study was to gather the knowledge and experience of the RS community regarding the scaling problems in the context of ecophysiological monitoring, identify gaps, strengths, and weaknesses, and guide RS scientists who want to expand their research from vegetation biophysical properties to physiology.

2. Material and methods

2.1. The spatial scaling challenge

The Spatial Scaling Challenge (SSC) was organized by the coordinators of the SENSECO Working Group 1, 'Closing the scaling gap: from leaf measurements to

satellite images', who anonymized the identity of all participants in all cases and hid the problem 'solution' until participation was closed (Figure 1). The SSC was announced in April 2022 among various RS networks and research communities worldwide working on the retrieval of vegetation ecophysiological parameters. The datasets and documentation were published open-access through ZENODO. The main dataset (Pacheco-Labrador et al. 2022b) included airborne scene imagery (NetCDF files) and field data sets. The field ancillary data was provided in two CSV files: one containing the spatial data acquired in the field sampling plots and a second including the time series of NPQ and meteorological variables measured in a nearby Eddy Covariance tower. Matlab (.m), R (.R), and Python (.py) scripts were provided to import the SSC data, as well as to export the outcome results and products in a standardized format. Moreover, the SSC included template reports describing the retrieval and scaling methods applied to estimate each requested variable: C_{ab}, LAI, $V_{max,25}$, and NPQ. The SSC also provided a bonus dataset (Pacheco-Labrador et al. 2022a) that included a half-hourly time series of down-welling spectral irradiance (W m^{-2} μm^{-1}) in the visible and near-infrared domains as measured by a field spectroradiometer operating in a nearby ecosystem station. The information provided in the reports was complemented later with a questionnaire (supplementary material S1). The SSC contributors and SENSECO members collaborated to evaluate the results and obtained the conclusions presented in this manuscript (Figure 1).
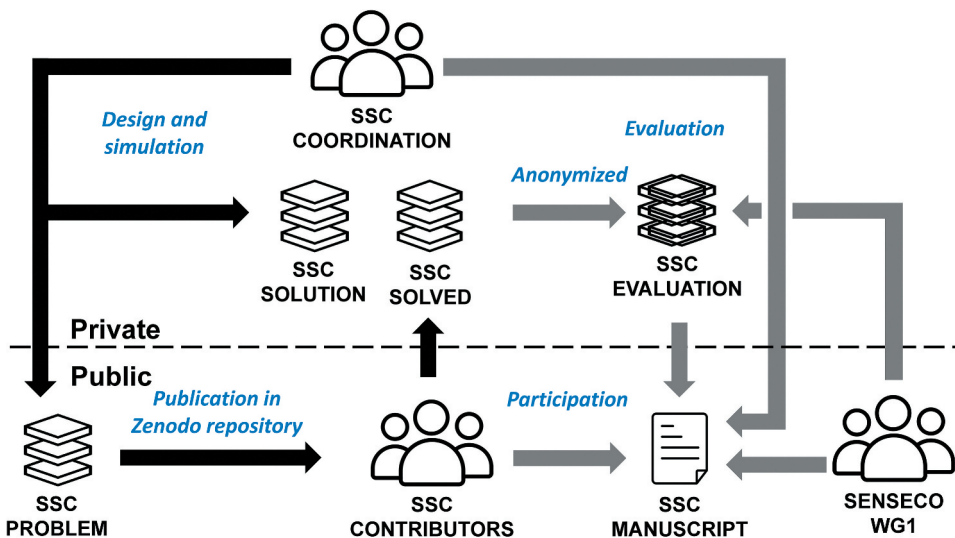
Figure 1. Spatial scaling challenge (SSC) workflow. The SCC coordinators designed and simulated the different SSC datasets privately, and published the 'problem' dataset in a zenodo repository. The contributors 'solved' the SSC and sent their contributions to the SSC coordination. These evaluated their results, anonymized them, and shared them with the participants and other COST action CA17134 SENSECO working group 1 collaborators for the elaboration of the manuscript, some of which contributed to evaluating some of the anonymized results.

2.2. Scene simulation

Except for the meteorological variables provided by an automated weather station in Spain, all the variables were synthetic, i.e. produced artificially with models and empirical equations and sampled from a normal distribution with assigned means and standard deviations. Despite their synthetic nature, those values throughout the manuscript are referred to as ground truth, reference data, baseline dataset, and measured data. This section provides a comprehensive overview of what parameters were modelled and the principles behind them. For a more thorough exploration, please consult the supplementary materials S2 (Supplementary S2.1 and Table S2.1). The SSC simulated two crop fields, maize (*Zea mays* L.) and wheat (*Triticum aestivum* L.), in different growth stages. The fields were exposed to varying fertilization and soil moisture gradients. The scene was 100 m × 100 m, with a bare soil corridor separating the fields. Meteorological data from Majadas de Tiétar was used for the simulation, which took place during the summer under high radiation and vapour pressure deficit conditions. The SSC campaign simulated ground sampling and airborne imagery datasets with the Soil Canopy Observation, Photochemistry and Energy model (SCOPE, v1.73) (van der Tol et al. 2009).

2.2.1. Water and nutrient availability treatments

The simulations comprise two crop management treatments. The first was a biochar amendment with a nitrogen enrichment along the fields' North–South (NS) axis (Fig. S2.1), which reduced albedo (Fig. S2.2) and increased nitrogen availability. Over the long term, it influenced the vegetation properties, such as leaf area index, maximum carboxylation rate, and pigment content. The second was a drip irrigation system that created varying soil moisture zones within each field shortly before the campaign, inducing physiological fast stress responses along the East–West (EW) direction (Fig. S2.3). Smooth soil moisture transitions between water regimes were simulated using log functions. Biochar also positively impacted soil water retention.

2.2.2. Soil properties and soil moisture stress simulation

The soil input variables of the Brightness – Shape – Moisture (BSM) model of SCOPE (Verhoef, van der Tol, and Middleton 2018) were spatially defined, with Gaussian noise added to simulate natural variability. Some soil properties, such as soil brightness, field capacity (FC), and moisture content (SMC), were affected by fertilization and water treatments. A decreasing relationship between the relative soil water content (SMC/FC) and the soil resistance for evaporation from the pore space (r_{ss}) was defined to reduce soil evaporation under low moisture. In contrast, soil thermal emissivity was modulated based on SMC to modify energy balance and heat stress (Table S2.1, Table S2.1.3.1).

2.2.3. Vegetation input variables and stress-based radiative transfer modelling

The simulations modelled vegetation parameters based on crop-specific literature. Taxonomy, soil moisture, and nitrogen availability were the key drivers of the vegetation spatial variability of properties and physiological state (Table S2.1, Table S2.1.4.1). Most vegetation properties such as foliar nitrogen content, leaf dry matter content, pigment contents, the leaf structural parameter, $V_{cmax,25}$, LAI, or canopy height were simulated as a function of nitrogen fertilization or nitrogen-dependent variables (Fig S2.4-7). Other

variables, such as leaf angle distributions, stomatal sensitivity, fluorescence quantum efficiency, and photosystem II-to-I ratio, were estimated or adopted from the literature. The rate coefficient of non-photochemical quenching was modelled as a function of relative light saturation and soil moisture content (Fig. S2.1.4.1, S2.8). Gaussian noise was added to simulate natural variability in all variables.

2.2.4. Airborne campaign

The simulations modelled airborne hyperspectral optical and thermal imagery acquisition over a simulated scene. The virtual flight took place at midday (11:45 UTC, 13:45 local time) under specific conditions of solar radiation, temperature, and vapour pressure deficit. Three hyperspectral sensors were used, similar to the HyPlant+TASI system (Hanuš, Fabiánek, and Fajmon 2016; Siegmann et al. 2019). Simulated hemispherical-directional reflectance factors (HDRF, Fig. S2.9–11) and outgoing thermal radiance in the observation direction of each pixel were convolved to the spectral characteristics reported for the visible to near-infrared and shortwave infrared (VNIR + SWIR module) as well as the thermal imaging spectrometers. Fluorescence radiances (Fig. S2.12–13) were provided in the O_2-B and O_2-A bands (F_{687} and F_{760}, respectively). LST was retrieved using the TES algorithm (Hanuš, Fabiánek, and Fajmon 2016) from the bottom of the atmosphere radiances simulated by SCOPE (Fig. S2.14). Uncertainty levels were considered realistic based on previous studies (Table S2.1.5.1). All signals were simulated at 1 m spatial resolution, then degraded for fluorescence (4 m) and thermal (2 m) radiances. LST was retrieved from the 2 m resolution imagery.

2.2.5. Ancillary data from a field campaign

During the simulated flight campaign, we modelled vegetation sampling at various times. C_{ab}, LAI, $V_{cmax,25}$, and NPQ were measured at nine points in each field. A randomized sampling scheme was employed to minimize bias (Figure 2a). Measurements were conducted at different times to account for temporal discrepancies and limitations in
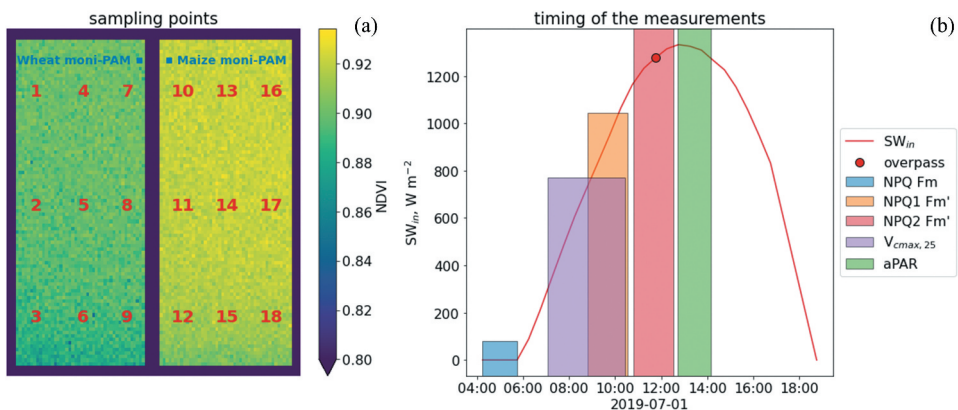
Figure 2. (a) Location of the field sampling plots and permanent moni-pam. (b) Temporal distribution of the different measurements (time ranges) and incoming shortwave incoming radiation (SW_{in}). The time on the x-axis is in UTC, local time was UTC + 2, taking the flight one hour before maximum solar height.

instrumentation and personnel. This resulted in a temporal mismatch between airborne and field sampling, potentially impacting physiological variables that fluctuate throughout the day.

Ten top-of-canopy leaves were measured using a chlorophyll metre. The readings were converted into C_{ab} using a calibrated model. The combined measurement and model uncertainty for each leaf measurement was 5%. LAI was estimated through destructive sampling after the campaign, with an assumed negligible uncertainty of 1.5%. LAI and C_{ab} were assumed to have no vertical variation, while $V_{cmax,25}$ and NPQ exhibited such variability. To simulate top-of-canopy leaf measurements, we averaged variables from the top 20 layers of the canopy model, introducing a bias.

$V_{cmax,25}$ was simulated using the SCOPE 'Vcmo' variable, an input of the model. A 2.5% relative uncertainty was assigned to $V_{cmax,25}$, assuming a single gas exchange chamber measurement. NPQ was calculated using fluorescence variables from Pulse Amplitude Modulation (PAM) measurements. Two rounds of NPQ measurements were simulated, from 10.50 AM to 12:30 PM and from 12:50 PM to 2:30 PM (local time). Continuous NPQ measurements were also simulated using monitoring PAM sensors (Figure 2a). These monitoring PAM sensors provided a reference for how NPQ changed over time. Still, they could not represent the entire fields because they were located in areas that were heavily fertilized. Wheat was irrigated in these areas, but maize was not getting enough water. We assumed that the relative uncertainties were 2.5%.

Ceptometer measurements were simulated to provide information on the absorbed PAR. The simulations aimed to investigate how participants would address uncertainties and mismatches between airborne and field data.

2.3. Analysis of the SSC contributions

2.3.1. Water and nutrient availability treatments

We considered four different aspects when evaluating each participant's contribution: (1) the retrieval method, namely parametric regression (PR), non-parametric regression (NPR), physically based (PB), and hybrid regression (HR) (Verrelst et al. 2015); (2) the predictors used to estimate each variable, such as HDRF, F_{687}, F_{760}, LST, VI, C_{ab} estimates, protein content estimates and meteorological conditions (W_X); (3) the use or omission of field measurements for constraining, fitting or training the retrieval method; and (4) the provision or omission of uncertainty maps for every retrieved variable. To perform this analysis, we created an anonymized dataset gathering all the contributions to the SSC. The items described above were identified in each submission based on i) the SSC description of the methods' report, ii) the complementing questionnaire, and iii) the results provided by each participant.

In the discussion, we considered to what extent the different contributions had accounted for spatial and temporal-scale mismatches when linking RS and field datasets, hence addressing the scaling issues. We also assessed how participants detected and interpreted early vegetation stress from the provided simulated data and/or their estimations of ecophysiological traits. Synthesis of these findings enabled us to draw recommendations addressing spatial scaling of spectral signals and properties related to vegetation's biophysical and physiological states. All this information was summarized in a single table (supplementary material S3) for analysis.

2.3.2. Statistical and performance analyses

The estimates from every contributor were compared with the corresponding simulated variables (Sect. 2.2), i.e. inputs or outputs of the model SCOPE labelled as the benchmark dataset (BD). First, the distribution of the retrieved estimates was compared using violin plots to understand the general patterns provided by each method in every crop. Then, Taylor plots were then applied to assess how well the different contributions reproduced the BD without distinguishing vegetation types. These plots consist of a reference point representing the observed value, accompanied by the standard deviation of the observed and model values. The model outputs were plotted in the diagram, with the distance from the reference point indicating the root-mean-square difference between the model and the observations after 'centralisation' in the units of the standard deviation of the measured data. The angle represented the correlation or similarity in spatial patterns between the model and the observations. Finally, a statistical analysis with *RMSE* (Root Mean Square Error) and Spearman's Rank Correlation (ρ) was carried out to compare estimates and simulations separately per field.

3. Results

3.1. SSC participation, methods and approaches

The SSC received 15 contributions from 13 groups or individual participants. NPR, followed by PR approaches, was most often used (Figure 3a). HR was never applied to estimate NPQ, which was mapped only in 13 contributions. The two former results suggest that NPQ was the most challenging variable for the participants to retrieve. The retrievals relied most often on reflectance factors, either the full spectrum (HDRF) or VIs, but *F* and LST were usually included (Figure 3b), particularly by NPR approaches (supplementary material S3) and for the variables linked to physiology ($V_{cmax,25}$, and NPQ). The estimates of $V_{cmax,25}$ and NPQ also involved the use of more predictor and ancillary variables across the approaches than LAI and C_{ab} (Figure 3c), mainly. For example, meteorological data was used to simulate vegetation physiological condition, and biophysical parameter estimates ($P_{RTM,est}$) such as C_{ab} and protein content were used both as predictors and inputs of physical models or indirectly as ancillary data in HR simulations. Among the NPR approaches, partial least squares regression (PLSR), an algorithm with a long history of usage in RS, was the most used (4/7). The other algorithms used (3/7) belong to the artificial intelligence family, which are becoming increasingly popular in RS as in many other fields: support vector machine (SVM), random forest (RF), and Gaussian process regression (GPR). PR, the most historically used approach in RS, predominantly involved simple or multiple linear regression models based mainly on VI and field data. The use of process-based models and inversion approaches requires deep, specific knowledge of the models' theory and inversion techniques. Those using PB retrievals relied on look-up-tables (LUT) generated with the Soil-Canopy Observation Photosynthesis and Energy fluxes (SCOPE v2.0), and the inversion was informed with previous estimates of biophysical variables (e.g. C_{ab} to estimate $V_{cmax,25}$ or NPQ). The HR approaches involved using PROSPECT-D or PROSPECT-PRO & the SAIL, or the SCOPE optical RTM simulations to train an NPR model (i.e. SVM, RF, and GPR) that, in turn, was used to estimate the variables of interest from HDRF. Only one HR participant used field data to constrain the variable
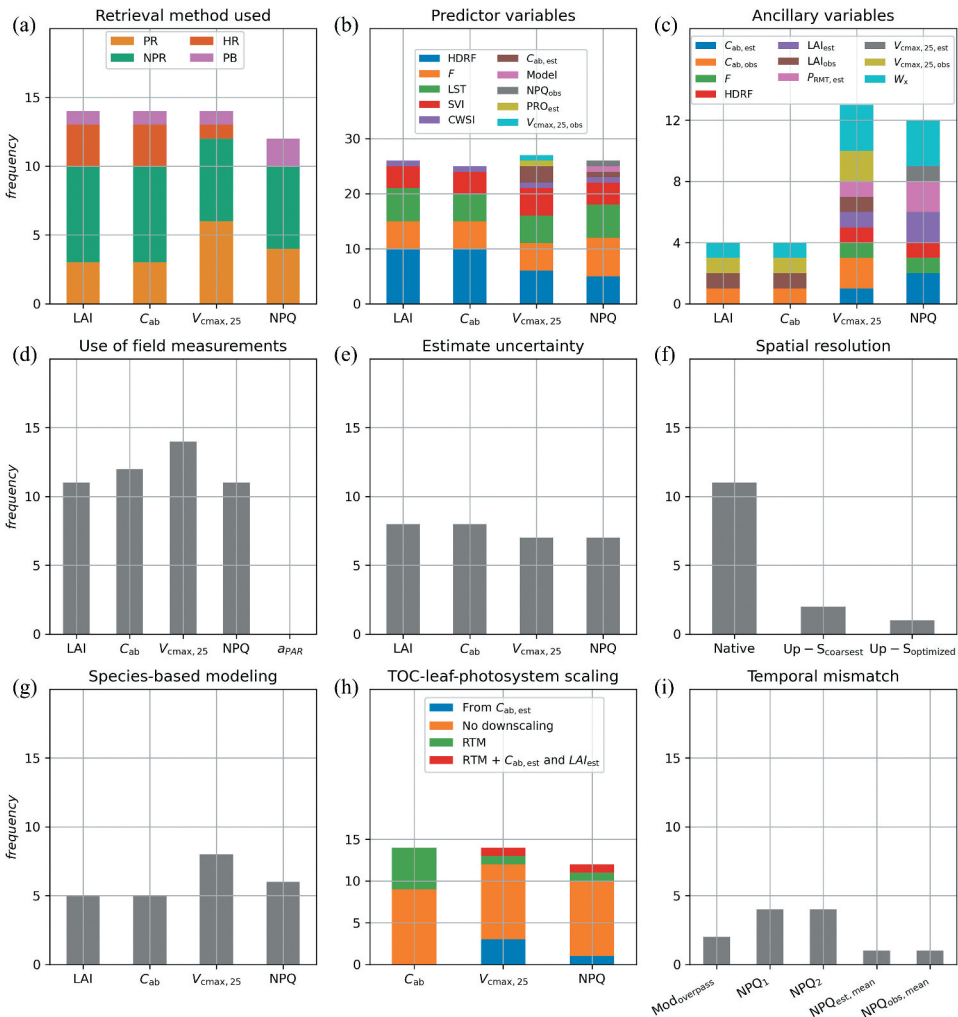
Figure 3. Summary of methods and input data used by SSC participants ($n = 15$). (a) Frequency of the different retrieval approaches (parametric regression (PR), non-parametric regression (NPR), physically based (PB) and hybrid regression (HR)) used to estimate leaf area index (LAI), leaf chlorophyll content (C_{ab}), maximal carboxylation rate ($V_{cmax,25}$), and non-photochemical quenching (NPQ). (b) Frequency of the predictor variables used to estimate each variable: reflectance factor (HDRF), sun-induced fluorescence radiance (F), land surface temperature (LST), vegetation indices (VI), crop water stress index (CSWI), estimated C_{ab} ($C_{ab,est}$), protein content (PRO_{est}), or LAI (LAI_{est}), a biophysical model (Model), observed $V_{cmax,25}$ ($V_{cmax,25,obs}$), or NPQ (NPQ_{obs}). (c) Frequency of use of ancillary information for estimating the different vegetation variables, including meteorological variables (W_x), spectral variables, or other estimated RTM variables regarding soil, leaf, or canopy properties (P_{RTM}) (d) frequency of use of the different field datasets. (e) Frequency of estimation of uncertainty for each vegetation variable. (f) Frequency of the approach adopted to deal with the different RS spatial resolutions (imagery used at native resolution (native), up-scaled to the coarsest resolution (Up-$S_{coarsest}$) or up-scaled using kriging (Up-$S_{optimized}$)). (g) Frequency of use of species/crop-specific models for the retrieval of each vegetation variable. (h) Frequency of approaches used to explicit the change of scale from top of the canopy (spectral information) to leaf (i.e. C_{ab} and $V_{cmax,25}$) or photosystem (NPQ) levels: no down-scaling is explicit (no downscaling), radiative transfer models (RTM) and/or estimates of C_{ab} ($C_{ab,est}$), or LAI (LAI_{est}). (i) Frequency of approaches used to consider or not the temporal mismatch between the acquisition of RS and NPQ data: using models informed with meteorological data at the time of the overpass (Mod$_{overpass}$), averaging field NPQ observations acquired at different times of the day (NPQ$_{obs,mean}$), or NPQ sampled in the early (NPQ$_1$) or the late (NPQ$_2$) morning.

ranges of the simulations (see supplementary material S3 for summarized information regarding each retrieval approach). All the field vegetation measurements provided were used at some point by the participants except absorbed PAR (aPAR) (Figure 3d), among which $V_{cmax,25}$ was the most often used. Approximately 60% of the contributions provided maps of estimated uncertainties (Figure 3e), most commonly generated via model ensembles (6/10), followed by GPR or Bayesian inference (2/10), and the model fit RMSE (2/10). However, none of the participants accounted for the reported uncertainty of the field datasets for fitting or inverting models. One of the HR approaches (#2) added noise to the simulated spectral variables to reduce overfitting, which is highly recommended based on previous experiences.

Regarding the spatial challenges, most participants used RS data at the native resolution when combining imagery of different pixel sizes (Figure 3f). In two cases, the imagery was up-scaled (down-sampling) to the coarsest resolution, and one explored different resolutions for Kriging. None of the participants attempted to sharpen the coarsest imagery. The predominant use of data-hungry NPR approaches limited the modelling of maize and wheat crops separately (Figure 3g). Separated models were most often used by PR approaches for which it is hard to capture complex patterns, and, in one case, by NPR. All the PB and HR approaches using the SCOPE2.0 model (P. Yang et al. 2021) accounted for the canopies' different photosynthetic pathways (C3 or C4) to retrieve/simulate physiological variables.

When estimating leaf or photosystem-scale variables from TOC spectral information, a distinction is made between purely statistical models, which do not explicitly consider scaling effects, and PB and HR approaches embedding the down-scaling in the RTM formulation. While most contributions were data-driven, a few cases included plant traits at canopy (i.e. LAI) and leaf (i.e. C_{ab}) scales as predictors of $V_{cmax,25}$ and NPQ (Figure 3h). Such traits provide information below the remote sensor resolution (particularly C_{ab}), adding therefore scale information to the empirical approaches. Finally, the participants faced the temporal mismatch between the field measurements of NPQ through the diurnal cycle and the sensors' overpass time. Surprisingly, more participants used the NPQ measurements acquired before (NPQ_1) than around the (NPQ_2) overpass time, which were, therefore, less related to the spectral signals captured by the remote sensors (Figure 3i). Two participants averaged observations or estimates of both datasets and two simulated NPQ with SCOPE using the meteorological conditions of the overpass.

3.2. Statistical and performance analyses

3.2.1. Evaluation of estimate's distributions

NPR-estimated LAI distributions were comparable to those of the benchmark dataset (BD, Figure 4a). The contributions (#5, #6, and #12), which used all the available information (HDFR, F, LST, and field data) presented more similar distributions than those using only HDRF and field data (#3 and #15). The only exception (#10) might be due to a potential overfit of the RF model used to predict LAI. PB (#11) and HR (#14), which exclusively used HDRF, achieved the least comparable distributions. The PR based on VIs achieved relatively comparable distributions; however, in one case (#8), the models provided a highly biased maize LAI estimate.
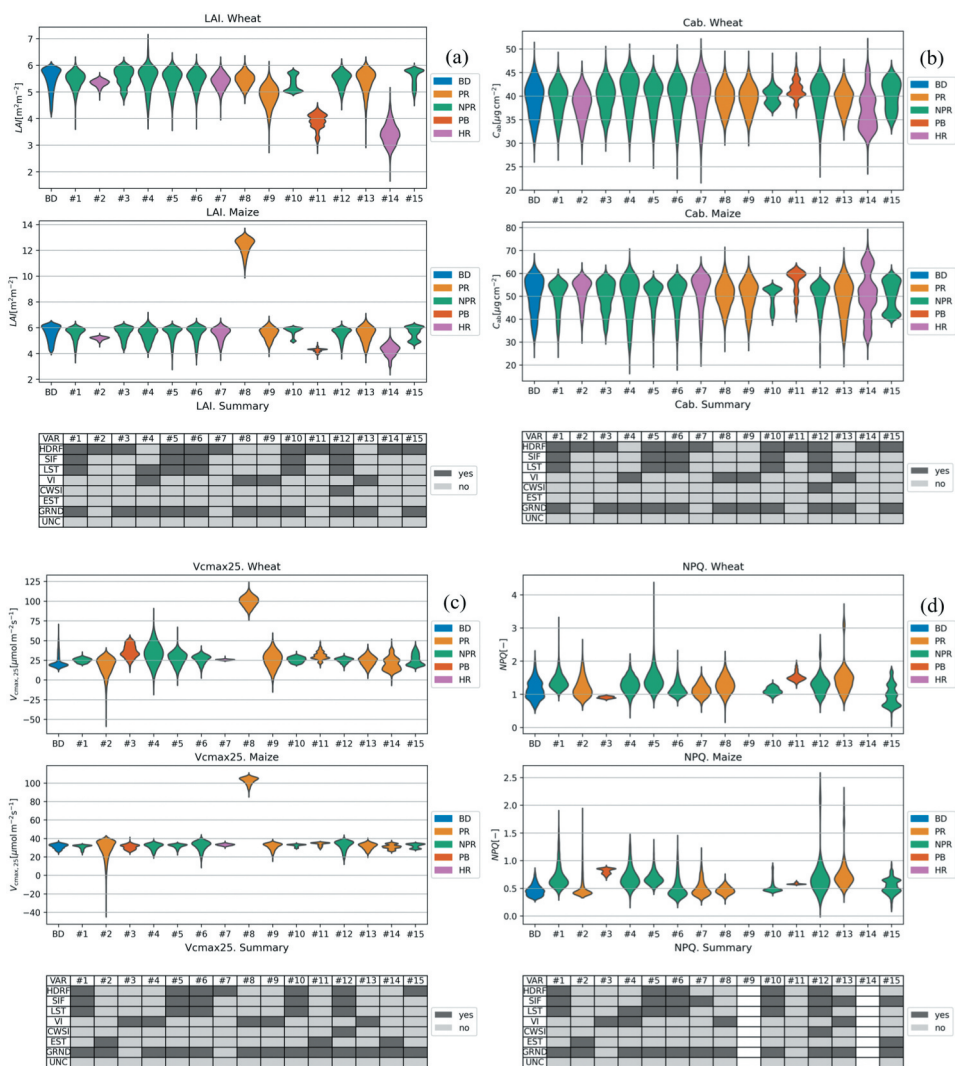
Figure 4. Comparison of the data distribution for the model simulations relative to the pseudo observations for (a) leaf area index (LAI), (b) leaf chlorophyll content (C_{ab}), maximum (c) carboxylation rate at optimum temperature ($V_{cmax,25}$) and non-photochemical quenching (NPQ). The colours separate the baseline dataset (BD) from the retrieval method types: parametric regression (PR), non-parametric regression (NPR), physically based (PB), and hybrid regression (HR). The summary table below each violin plot summarises: 1) what were the predictors/constraints of each model, including hemispherical-directional reflectance factors (HDRF), solar-induced fluorescence radiance (F), land surface temperature (LST), vegetation indices (VI), the crop water stress index (CWSI), estimates of biophysical variables (EST, such as (C_{ab}), protein content, or LAI). 2) whether the models used field data to fit models or as ancillary information (GRND). 3) whether the contributors accounted for the reported uncertainty of the field observations during training or retrieval (UNC).

Most participants obtained consistent C_{ab} estimates (Figure 4b), except PB (#11) and an NPR where the RF might not have been properly trained (#10). NPR led to distributions closer to BD, whereas PR provided slightly less skewed estimates. The HR cases that either added random noise to train the statistical model (#2) or used field data to constrain the

ranges of the simulations (#7) obtained acceptable distributions, while the case that did not (#14) produced bimodal distributions, which might indicate overfitting during the training of the statistical model.

The distributions of $V_{cmax,25}$ estimates were less comparable to BD than LAI or C_{ab} (Figure 4c). While most were close to the BD ranges, as with LAI, contribution #8 (PR based on VIs) largely overestimated $V_{cmax,25}$ in both crops. In contrast, contribution #2 (HR) obtained a long-tailed distribution with large negative values. Other PR and NPR contributions also provided negative estimates. Overall, estimates were more comparable for maize than wheat. NPQ distributions were the least comparable with BD (Figure 4d). However, contribution #8 (PR based on VIs) obtained the closest distribution to maize BD and was comparable for wheat. Contributions using PB (#3, #11) and an NPR where the RF might not have been properly trained (#10) provided estimate ranges that were too narrow, and the PB estimates were particularly biased. On the contrary, some NPR (#1, #12) and PR (#2, #13) presented wide distributions with a few overestimated values for both fields. In all cases, the biases are not related to the fact that the participants used the early NPQ dataset (NPQ1). This suggests the uncertainty comes from the models' formulation or inversion inability to adequately capture the relationships between spectral and other information and NPQ.

3.2.2. Models' performance

Figure 5 Taylor plots show that C_{ab} estimates were the most correlated with BD, with centred RMSE around 0.60 standard deviations (σ). LAI Pearson correlations (r) are distributed towards lower values with errors RMSE centred around 0.80σ. $V_{cmax,25}$ featured the lowest r, but most estimates cluster around $r \sim 0.80$ and RMSE $\sim 0.75\sigma$. NPQ estimates present two differentiated clusters, the first with $r \sim 0.90$ and RMSE $= 0.50\sigma$, the second with $r \sim 0.75$ and RMSE $\sim 0.57\sigma$, and a single point with $r < 0.40$ and RMSE $\sim 0.90\sigma$. Overall, $V_{cmax,25}$ featured the largest variability of performances.

NPR approaches achieved the lowest errors and strongest correlations (Figures 6 and 7). NPR used a larger and more diverse number of predictors than the rest of the methods (supplementary material S3), which might increase robustness against observational uncertainties and reduce overfitting. PR and PB showed the largest RMSE discrepancies between the different crops, suggesting they can be very specific (PR) or case-dependent (PB). Compared to the measurement uncertainties of the variables in the field, estimated *RMSE* were ~8.1 (LAI), ~1.1 (C_{ab}), ~15.8 ($V_{cmax,25}$), and ~12.3 (NPQ) times larger (supplementary material S4, Table S4.1).

3.3. Long-term and short-term stress detection

3.3.1. Long-term biophysical stress responses (NS gradient)

The NS Nitrogen availability gradient (Fig. S3.1) was detected by most contributors and identified as 'continuous' or 'long-term' (e.g. #4, #5) stress. Most contributors found higher productivity and biomass in the north, decreasing towards the south, based on the retrieved C_{ab} and LAI variables (#1, #3, #4, #5, #6, #7, #8, #9, #12) (supplementary material S4, Fig. S4.1. & S4.3). The causes of LAI and C_{ab}
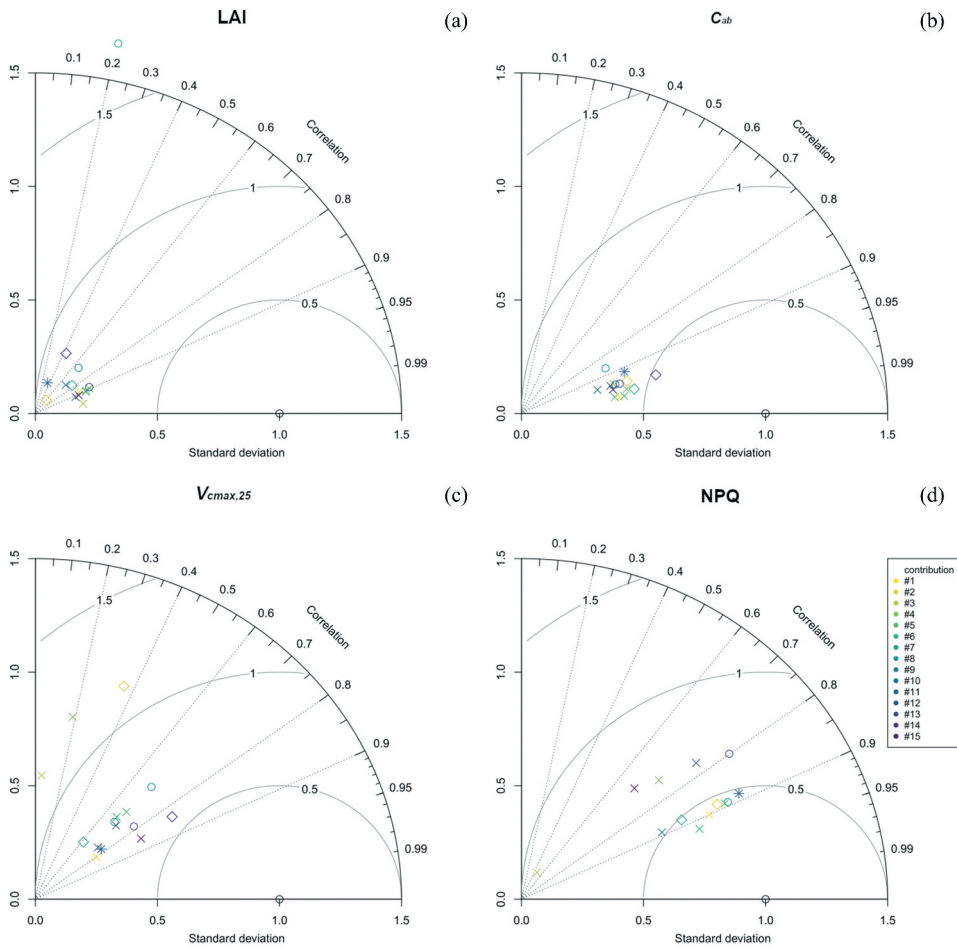
Figure 5. Taylor plots comparing simulated and estimated LAI (a), C_{ab} (b), $V_{cmax,25}$ (c), and NPQ (d). Each code corresponds to the SSC participants' contributions ranging from 1 to 15. The symbols identify the retrieval approach ('o' parametric regression, 'x' non-parametric regression, '*' physical; y-based, and '◇' hybrid regression).

variability were generally attributed to slower growth associated with different soil types having lower nitrogen and water content towards the south (e.g. #5, #7, #8, #9, #12). Heterogeneous soil conditions could also explain such gradients (#12).

In addition to the LAI and C_{ab} gradients, the NS stress trend was also reported based on $V_{cmax,25}$, and NPQ, as shown in Fig. S4.5. & S4.7. (e.g. #1, #5, #6, #8, #9). Higher LAI, C_{ab}, and $V_{cmax,25}$ values were considered to be closely related and linked to the plant nutrient status (#13, #14), and the NPQ trend was described as 'inverse' to the others (e.g. #1, #6) if detected. In general, it was reported that the maize field NPQ did not show any spatial gradient, unlike wheat (#12). In addition, #10 detected an NS gradient in the Water Deficit Index (WDI) (Moran et al. 1994), an index developed to detect crop water deficit using surface–air temperature difference and a spectral vegetation index (NDVI), also revealed an NS gradient (#10).
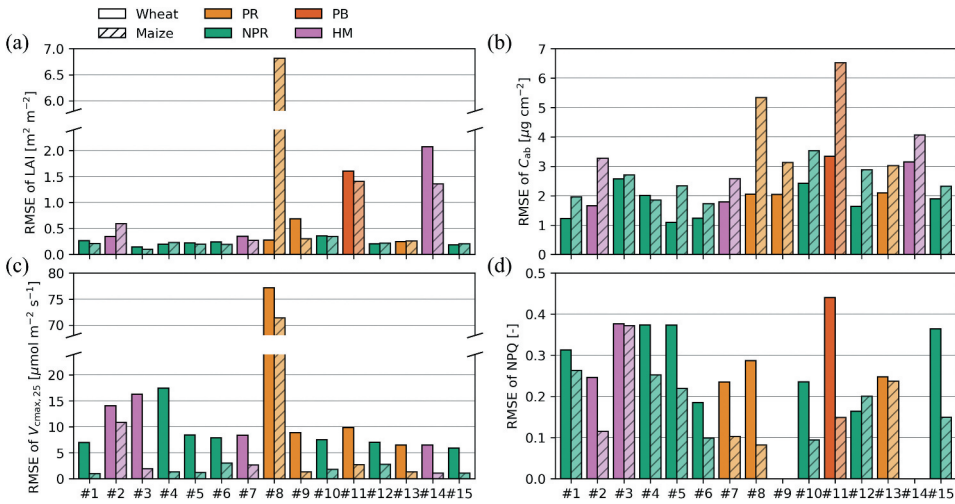
Figure 6. Root mean squared error (RMSE) between simulation and estimation for (a) LAI; (b) C_{ab}; (c) $V_{cmax,25}$; and (d) NPQ. Colours are based on the method type (similar to fig. 4), and the texture of the bars refers to the vegetation type. Note that in panel (a), the y-scale was truncated to improve the visibility; the RMSE for maize of model #8 is 6.82 $m^2\ m^{-2}$.
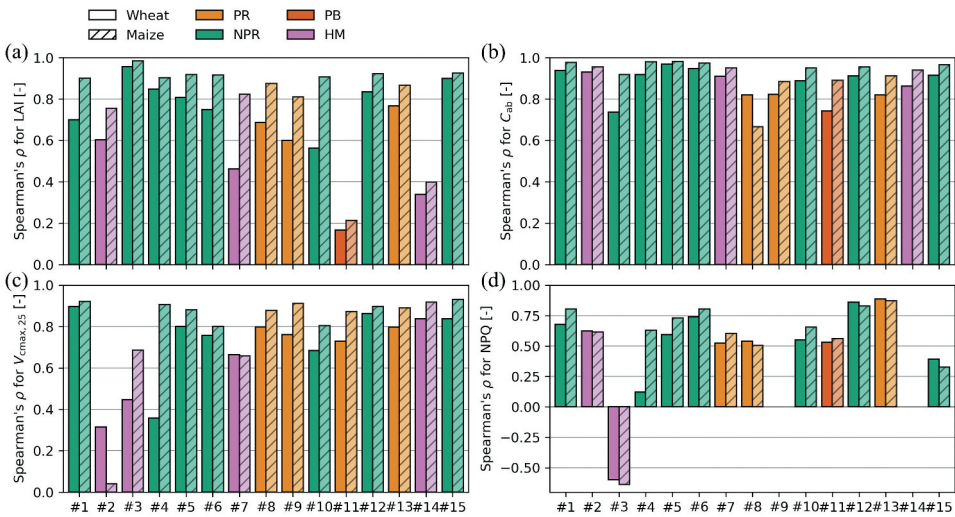
Figure 7. Spearman's rank correlation (ρ) between simulation and estimation for (a) LAI; (b) C_{ab}; (c) $V_{cmax,25}$; and (d) NPQ. Colours are based on the method type (similar to fig. 4), and the texture of the bars refers to the vegetation type.

3.3.2. Short-term acute physiological stress responses (EW gradient)

The decreasing EW soil moisture content gradient (Fig. S2.3) proved more difficult to detect and was only reported by a few participants through the patterns observed in the retrieved NPQ (#13, #14) or the F imagery (#4) (Fig. S4.7). Specifically, the use of F relied on F_{687} normalized by sunlit leaf area ($F_{687,sl}$, obtained by retrieving leaf angle distribution factors from the SCOPE model first, then calculating the sunlit leaf area by using the

retrieved LIDF values), assuming aPAR is the main factor dominating the F signal. A few participants also used a combination of parameters/methods (#3, #4, #10) to produce stress maps (Fig. S4.9). The fluorescence yield ($F_{687,sl}$) obtained after post-processing the F_{687} values showed an EW gradient, as did the combined ($V_{cmax,25}$, NPQ, and nadir-normalized $F_{687\text{-yield}}$ and $F_{760\text{-yield}}$) stress map (#4). It was also pointed out that the fluorescence yield maps showed the EW but not NS stress gradients.

The EW stress gradient was attributed to acute or management-driven stress (#4). Although a few methods were adequate to assess EW trends or soil moisture zones, several reports differentiated between long-term (nutrient status) and acute (heat, drought) stress effects, and the output maps were considered as a result of the combinations of both (#5, #6, #7, #8, #9, #10 #11, #12).

3.3.3. Stress detection across species

Differences were found between maize and wheat stands under stress conditions, as observed in both the F imagery and derived variables such as $F_{687,sl}$ (#4), LAI, C_{ab}, $V_{cmax,25}$, and NPQ maps (#4, #5, #6). Additionally, distinctions were evident in the LST imagery (#5, #6, #7, #12) and a water deficit index (#10). The stand differences were also evident in the derived relationships and normalized signals that the participants were able to interpret. Maize was found to be generally less stressed than wheat, based on relationships between NPQ and nadir-normalized $F_{687,nadir}$ values (Hao et al. 2022) and from the lower nadir normalized $F_{760,nadir}$ values seen in wheat compared to maize. It was also reported that wheat plants experienced more stress than maize due to their C3 photosynthetic pathway. Maize, being a C4 plant, exhibited a higher light compensation point (#13), temperature tolerance (#5, #6, #7, #12, #13), and water use efficiency (#12). The increased stress level in the case of the wheat stand was found by the participants to be accompanied by increased variability or lower estimation accuracy of $V_{cmax,25}$ (#5, #7, #8, #9), while on the contrary, maize showed a less variable and higher photosynthetic performance (#5, #6, #12) irrespective of the daytime high radiation and temperature.

4. Discussion

4.1. Addressing the scaling challenges

The SSC asked the RS community to estimate four variables – LAI, C_{ab}, $V_{cmax,25}$, and NPQ – featuring different effects on vegetation optical and thermal spectral properties and different spatial and temporal scales of variability. Beyond the performance evaluation, the SSC sought to assess to what extent and how the participants addressed the different scaling problems. Since these scaling issues already limit the exhaustive measurement of these variables in the field, the SSC relied on detailed simulations of RS and field observations to generate a dataset that enabled an adequate assessment of the results. While we acknowledge that the simulation framework produced simplified representations that can be biased or less challenging than the real world, we consider the SSC dataset sufficient to assess the degree of understanding and consideration of the scaling issues performed by participants. In particular, we simulated different stress types linked to vegetation properties and functioning using relationships previously reported in the

literature. In addition, we included randomness originating from the natural variability of individuals in all vegetation variables and uncertainties related to all simulated measurements. The specificities of these relationships and the model SCOPE v1.73 selected for conducting the simulation could bias estimates relying on PB models (i.e. SCOPE2.0 (P. Yang et al. 2021) and different versions of PROSPECT (J. B. Féret et al. 2017; J.-B. Féret et al. 2021) + SAIL (Verhoef 1984)), featuring different assumptions or representations of vegetation and related signals.

4.1.1. Methods

NPR models were most used and achieved lower relative RMSE values than the rest of the approaches (~15% (LAI), ~62% (C_{ab}), ~64% ($V_{cmax,25}$), and ~98% (NPQ)). However, these flexible but data-hungry algorithms were trained with relatively small datasets (9–18 field observations), likely at the expense of a lack of generalization (Verrelst et al. 2019; Wang, Guan, Wang, Ainsworth, Zheng, Townsend, Liu, et al. 2021). PR was the second most used approach, and unlike the others, it used only a small fraction of the information available. Still, these achieved acceptable performances in most of the cases. We hypothesize that the smoothness of the vegetation gradients favoured the performance of NPR and PR approaches, particularly when models were trained per species. In any case, the use of these models is limited to the availability of field data, which does not necessarily prevent extrapolation (e.g. Moreno-Martínez et al. (2018)). Alternatively, HR approaches only require knowledge of the forward use of a physical model since inputs and outputs are integrated into an NPR model. HR was used more than PB and often performed better, but not as well as NPR. One of the sources of uncertainty for PB and HR is the discrepancy between the model and reality (or, in this case, the model used for the simulations). For example, contributor #2 used PROSPECT-PRO (J.-B. Féret et al. 2021) RTM to estimate $V_{cmax,25}$ exploiting the absorption features of proteins in the leaf. However, the SCOPE simulations did not present such features, which could explain the low correlation obtained by #2 (Figure 7c). Nonetheless, this approach could perform better when applied to real vegetation measurements (e.g. Wang, Guan, Wang, Ainsworth, Zheng, Townsend, Li, et al. (2021), Camino et al. (2022)). While the number of contributions using PB and HR is too low to make clear conclusions, HR training error might relax the underlying assumptions of the physical model, improving, in some cases, the retrieval (Verrelst et al. 2019; Wang, Guan, Wang, Ainsworth, Zheng, Townsend, Liu, et al. 2021). Overall, better results were obtained when retrieving biophysical parameters with a strong effect on the optical signals (i.e. LAI and C_{ab}) than the two physiological variables indirectly related to F, LST, and PRI (i.e. $V_{cmax,25}$, and NPQ) (Figures 5–7). Our results demonstrate that modelling and data assimilation improvements are needed to adequately characterize plant physiological variables from RS, particularly when no field data is available to calibrate empirical models. Finally, none of the contributors used the observational uncertainties of the field measurements nor asked about the uncertainty estimates of RS imagery. Uncertainties could have been employed to assign weights to each data point's contribution during model training and to subsequently propagate these uncertainties to the predictions. Uncertainty maps were exclusively generated based on the models' fitting errors (Porwal and Raftery 2022).

4.1.2. Scaling challenges

The SSC presented several spatial challenges. The first one was the heterogeneity of spatial resolutions in the RS imagery. The spatial resolution is relevant for the retrieval of vegetation ecophysiological properties since these relate non-linearly with the spectral signals and unresolved heterogeneity (spectral mixture) increase estimation uncertainty (Pacheco-Labrador et al. 2022; Vicente et al. 2021). Maybe partly due to the smoothness of the simulated crop field, none of the participants attempted to downscale the imagery to the finest resolution, which might be more relevant in heterogeneous environments. Still, larger errors were found in the borders than in the interior of the fields, where bare soil and vegetation signals were mixed (supplementary material S4). While the down-scaling of reflectance factors (e.g. fusion of multi and hyperspectral imagery (Vivone 2023)) relies on univocal relationships between the data at different scales, the down-scaling of physiologically regulated signals transfer (e.g. PRI, or thermal and SIF emissions) is more challenging. The latest would require ancillary information (e.g. canopy structure driving SIF escape and current incoming PAR) and accounting for the diurnal and seasonal dynamics of these signals and their relationship with plant physiology. For example, Guzinski et al. (2020) used physical models to downscale evapotranspiration retrievals, whereas Duveiller et al. (2020) used LST and semi-empirical stress models to down-scale coarse global SIF products.

The second challenge was the species-dependent variability in the relationships between vegetation ecophysiological properties and the observed spectral signals for the vegetation types represented (i.e. wheat C3 and maize C4). This is particularly true for the C3 and C4 plants, which have developed different mechanisms to fix CO_2 from the atmosphere, resulting in differences in absorbing (LAI, C_{ab}), using ($V_{cmax,25}$), and disposing (NPQ) radiation (Table S2.1.4.1). Half of the SSC participants modelled both vegetation types separately. While the number of contributions did not allow for a complete under-standing of the impact of vegetation-type differentiation, previous studies show that it could improve the retrieval of ecophysiological properties (Moreno-Martínez et al. 2018). In the SSC, small sample sizes prevented most NPR approaches from characterizing each vegetation type separately. Such separation could be strongly recommendable for simple PR approaches that are unfit for generalization. In the case of PB and HR, physical models impose strong assumptions on the relationships between ecophysiological and spectral signals. However, radiative transfer theory offers different formulations (Widlowski et al. 2015), which could be selected as a function of the vegetation type (Wang, Guan, Wang, Ainsworth, Zheng, Townsend, Liu, et al. 2021). C3/C4 differentiation is inherent to phy-siological models often based on the Farquhar – von Caemmerer – Berry biochemical photosynthesis model. This must be accounted for by missions studying photosynthesis, such as FLEX, which aims to provide a light-response-centred approach for estimating photosynthetic efficiency (Liu et al. 2022) accounting for C3 and C4 vegetation types (ESA 2015). In all cases, vegetation type-oriented modelling relies on vegetation-type mapping, where the discrimination between C3 and C4 vegetation from RS remains particularly challenging (Poulter et al. 2015).

A third challenge was the spatial scale of each retrieved variable (i.e. photosystem, leaf, or canopy). LAI is a canopy variable with strong control over all spectral signals, whereas C_{ab} is a foliar variable with substantial radiation control in the visible spectral region. Both influence vegetation photosynthesis and transpiration via aPAR and gas exchange area.

On the other hand, $V_{cmax,25}$ is a foliar property with a weak manifestation in spectral signals (mainly in F). Finally, NPQ is not a vegetation property but a state that varies dynamically over time according to environmental conditions. SSC simulations only represented vertical profiles of $V_{cmax,25}$ and NPQ, and the participants were informed these had been sampled from the upper layers of the canopy. While the participants did not consider the vertical gradients when training models or evaluating their estimates, no systematic biases were found in the retrievals (Figure 4), which suggests other factors dominated uncertainties. PB and HR approaches embed the down-scaling from TOC to leaf (i.e. C_{ab}) or photosystem (i.e. $V_{cmax,25}$, and NPQ) level in the RTM formulations. However, the complexity of coupled physiological-RTM models accounting for environmental factors and vertical gradients within the canopy made the use of fully coupled models rare. Despite their complexity, these approaches performed worse than the empirical ones. In all cases, the retrieval of biophysical (LAI and C_{ab}) and physiological variables ($V_{cmax,25}$, and NPQ) was separated into two steps where the first estimates informed the retrieval of the second, an approach that can reduce equifinality in the retrieval of least influencing variables (Pacheco-Labrador et al. 2019). PR and NPR do not provide an explicit-scale transfer. However, they can include biophysical variables relevant to the change of scale as predictors. Whereas LAI estimates did not support the retrieval of C_{ab}, LAI or C_{ab}, and even protein content estimates became predictors of $V_{cmax,25}$ or NPQ. A second alternative could be to jointly model variables of different scales to exploit potential covariances, reducing equifinality and maybe providing more consistent estimates.

The fourth challenge relates to the temporal mismatch between vegetation between variables and spectral observations. LAI and C_{ab} were simulated as being static in time, as intra-daily variation is usually neglected. $V_{cmax,25}$ measurements were simulated under conditions similar to those inside a leaf chamber. However, it must be considered that the actual carboxylation rate achieved by the plant is variable, which can bias the relationship between $V_{cmax,25}$ and spectral signals influenced by physiology (i.e. F, PRI, and LST) over time, the links not necessarily being coherent. NPQ is highly dynamic; two datasets were provided: the first prior to the flight (NPQ_1) and the second centred around the overflight time (NPQ_2). Despite this temporal mismatch being most often disregarded, no systematic biases were found for the contributions using NPQ1, suggesting that the retrieval drives uncertainty.

4.2. Stress assessment

SSC considered three types of stress: (1) long-term nitrogen limitation (NS), resulting in slow plant responses; (2) short-term water limitation (EW), resulting in fast plant responses; and (3) inherent differences between wheat and maize due to different photosynthetic pathways. In SSC, changes in growth responses were more easily detected by the different retrieval methodologies of common biophysical variables than physiological stress.

Plants balance the extent or size of roots and canopy and regulate the biosynthesis of photosynthetic pigments and the chlorophyll-to-carotenoid ratio in response to the long-term deficit of water or nutrient availability (Ru et al. 2023; Song et al. 2023). The long-term nitrogen-induced stress was evident in maps of retrieved variables with decreasing

values of LAI, C_{ab}, $V_{cmax,25}$, and increasing values of NPQ from N to S, which were coherent with the simulated nutrient availability (Fig. S3.1). Most contributors identified the simulated long-term nutritional stress via the retrieved biophysical variables.

Early stress induced by a sudden change in soil moisture content was evident in the provided airborne imagery: F_{687}, F_{760}, and more subtly PRI (Fig. S2.12, S2.13 and S2.11, respectively) presented clear EW stripe patterns (Fig. S3.3) despite being superimposed to the nutrient-stress induced patterns of LAI, C_{ab}, $V_{cmax,25}$, and other variables. Nonetheless, the SSC simulated two relatively homogeneous crop fields, facilitating the interpretation, which could be more complex in natural ecosystems. Short-term stress was also evident in the NPQ (Fig. S2.8) was collected in the field at several locations. However, these patterns were unclear in the estimated NPQ maps (Fig. S4.7) and were less often identified. In a few cases, the spatial patterns of F or corrected versions were related to stress. Furthermore, NPQ retrieval errors did not systematically relate to the fact of not taking into account spatial and temporal mismatches. These results suggest that despite RS signals being able to identify differences in physiological stress, we still lack suitable methods for retrieving physiological variables that disentangle such information from the rest of the biophysical and structural factors affecting the RS signals. The standardization of the collected data and field sampling (e.g. F and NPQ) to a common measurement time and the F post-processing towards fluorescence quantum efficiency (f_{qe}) maps (Moncholi-Estornell et al. 2023; Wieneke et al. 2024) could contribute to overcoming the retrieval challenges.

In the case of drought stress and different responses by C3 and C4 plants, plant hormone-driven (abscisic acid-mediated) stomatal closure is considered the first acclimation response with an immediate decrease in canopy evapotranspiration and an increase in surface temperature (Fahad et al. 2017; Zandalinas et al. 2018). However, the C3 and C4 plants differ in their drought tolerance due to different molecular, physiological, and developmental processes (Song et al. 2023), resulting in an altered sensitivity and timing of stomatal responses. This phenomenon was clearly detected in the wheat stand with a higher LST and a larger NPQ (in the field datasets NPQ_1 or NPQ_2) by the participants. The differences in F were also evident but were not used to discriminate drought tolerance between the two vegetation types. Despite the magnitudes being different, other biophysical parameters (e.g. LAI or C_{ab}) could challenge the interpretation of these differences, particularly when prior knowledge of the vegetation photosynthetic paths is unavailable.

The results regarding the interpretation and mapping of short-term stress suggest that expertise on this topic is less generalized than the study of biophysical properties of vegetation. The advent of new RS missions (e.g. FLEX, LSTM, CHIME, etc.) will increase the combination of different signals (e.g. F, LST and hyperspectral reflectance factors) and, therefore, the possibilities of assessing vegetation physiology from space. More specific training, open-source tools, and group collaboration will be necessary to extend this specific knowledge to a broader RS community.

5. Conclusions

In the context of the COST Action 'Optical synergies for spatiotemporal SENsing of Scalable ECOphysiological traits' (SENSECO) (CA17134), the SSC challenged the RS

community to down-scale and retrieve two biophysical and two physiological plant variables from a simulated airborne and field data and diagnose the vegetation stress.

Based on the SSC results and discussions held during the SENSECO COST Action activities, we have identified a number of areas where further research is necessary to foster operational down-scaling of biophysical/physiological variables as well as the early detection of vegetation stress. The following six prospective research areas of future work were summarized:

(1) *Synergetic multi-sensor detection of early stress and plant physiology characterisation*. Vegetation expresses these responses to an ever-changing environment at different rates in different spectral regions. Therefore, no single spectral variable can be expected to characterize the physiological status and reveal early stress completely. Methods for combining and assimilating RS images of different resolutions and quality, acquired at different times of the day, that are suitable to characterize plant physiology still need to be developed. The best option would be to use high-quality aerial and field datasets while addressing the subsequent considerations.

(2) *Accounting for the temporal dynamics of the physiological parameters or resulting plant status*. Light intensity and vapour pressure deficit regulate diurnal changes in leaf temperature, V_{cmax}, NPQ, fluorescence, and photochemistry, resulting in diurnal changes in *LTS, F*, and *PRI*. These changes must be considered when combining spectral information and vegetation variables in physical or empirical models or when comparing observations at different times of the day. Also, long-term stress (e.g. sustained NPQ) should be included in the modelling.

(3) *Accounting for the variability of biophysical/physiological parameters through the plant canopy vertical profile*. While optical and thermal RS imagery provides information about the upper canopy layers, the vertically varying environmental conditions within the canopy (light quality, wind speed, etc.) trigger different biophysical/physiological responses (e.g. C_{ab} and V_{cmax} profiles). This fact should be considered to determine vegetation status and/or early stress detection, particularly when top-of-canopy spectral information or field measurements of specific layers of the canopy are used to quantify or represent the whole vegetation's volume physiology.

(4) *Accounting for the spatial heterogeneity and intrapixel variability*. The inherent coarse resolution of most sensors able to capture physiologically driven signals makes the characterization of physiology particularly sensitive to the mixture of different surfaces, especially bare soil, inside a pixel (e.g. the SSC found large uncertainties in the crop boundaries). Such a mixture should be characterized and taken into account by physical or statistical models.

(5) *Down-scaling of spectral information from the top-of-canopy to the leaf and the photosystem levels*. Characterising the physiological status requires understanding vegetation properties at different scales where spectral information is either generated or transformed. Therefore, the interpretation of the spectral signals should be considered explicitly (physical models with the right formulations) or implicitly (empirical approaches, which can be supported by the inclusion of estimates of foliar and structural biophysical variables).

(6) *Accounting for uncertainties*. Solving the former steps involves combining different datasets for model inversion or fitting. However, not all the observations are equally valuable. Further efforts are needed to quantify and account for the observational uncertainties, minimize equifinality or biased predictions, and quantify the uncertainty of the estimated ecophysiological variables. This is fundamental to determine the level of confidence and the significance of the difference between two estimates (and, hence, the capability to discriminate stress).

Accounting for all these factors is demanding and requires deep knowledge. While very experienced research groups work and apply methods that comply with these needs, their use must be considered by less experienced researchers and popularized via open-access code or protocols that facilitate applying specialized data processing for the study of vegetation physiology from RS.

Disclosure statement

No potential conflict of interest was reported by the author(s).

Funding

ORCID

Javier Pacheco-Labrador http://orcid.org/0000-0003-3401-7081
M.Pilar Cendrero-Mateo http://orcid.org/0000-0001-5887-7890
Shari Van Wittenberghe http://orcid.org/0000-0002-5699-0352
Itza Hernandez-Sequeira http://orcid.org/0000-0002-1623-9337
Gerbrand Koren http://orcid.org/0000-0002-2275-0713
Egor Prikaziuk http://orcid.org/0000-0002-7331-7004
Szilvia Fóti http://orcid.org/0000-0003-3235-0948
Enrico Tomelleri http://orcid.org/0000-0001-6546-6459
Kadmiel Maseyk http://orcid.org/0000-0003-3299-4380
Nataša Čereković http://orcid.org/0000-0002-7195-5280
Rosario Gonzalez-Cascon http://orcid.org/0000-0003-3468-0967
Zbyněk Malenovský http://orcid.org/0000-0002-1271-8103
Mar Albert-Saiz http://orcid.org/0000-0001-5676-3750
Michal Antala http://orcid.org/0000-0003-1294-9507
János Balogh http://orcid.org/0000-0003-3211-5120
Henning Buddenbaum http://orcid.org/0000-0002-0956-5628

Joseph T. Fennell http://orcid.org/0000-0001-6874-6667
Jean-Baptiste Féret http://orcid.org/0000-0002-0151-1334
Miriam Machwitz http://orcid.org/0000-0002-4999-673X
Ádám Mészáros http://orcid.org/0009-0002-4971-3370
Guofang Miao http://orcid.org/0000-0001-5532-932X
Miguel Morata http://orcid.org/0000-0002-0537-6803
Paul Naethe http://orcid.org/0000-0002-3649-2786
Zoltán Nagy http://orcid.org/0000-0003-2839-522X
Krisztina Pintér http://orcid.org/0000-0001-8737-706X
R. Reddy Pullanagari http://orcid.org/0000-0001-6560-986X
Anshu Rastogi http://orcid.org/0000-0002-0953-7045
Bastian Siegmann http://orcid.org/0000-0002-1232-7102
Sheng Wang http://orcid.org/0000-0003-3385-3109
Chenhui Zhang http://orcid.org/0000-0003-3915-6099

Data availability statement

The data simulated in this work have been published in Open Access repositories.

References

Camino, C., K. Araño, J. A. Berni, H. Dierkes, J. L. Trapero-Casas, G. León-Ropero, M. Montes-Borrego, et al. 2022. "Detecting Xylella Fastidiosa in a Machine Learning Framework Using Vcmax and Leaf Biochemistry Quantified with Airborne Hyperspectral Imagery." *Remote Sensing of Environment* 282:113281. https://doi.org/10.1016/j.rse.2022.113281.

Damm, A., S. Cogliati, R. Colombo, L. Fritsche, A. Genangeli, L. Genesio, J. Hanus, et al. 2022. "Response Times of Remote Sensing Measured Sun-Induced Chlorophyll Fluorescence, Surface Temperature and Vegetation Indices to Evolving Soil Water Limitation in a Crop Canopy." *Remote Sensing of Environment* 273:112957. https://doi.org/10.1016/j.rse.2022.112957.

Del Río-Mena, L. W. Trinidad, G. Tsegay Tesfamariam, O. Beukes, and A. Nelson. 2020. "Remote Sensing for Mapping Ecosystem Services to Support Evaluation of Ecological Restoration Interventions in an Arid Landscape." *Ecological Indicators* 113:106182. https://doi.org/10.1016/j.ecolind.2020.106182.

Demmig-Adams, B., C. M. Cohu, O. Muller, and W. W. Adams. 2012. "Modulation of Photosynthetic Energy Conversion Efficiency in Nature: From Seconds to Seasons." *Photosynthesis Research* 113 (1): 75–88. https://doi.org/10.1007/s11120-012-9761-6.

Duveiller, G., F. Filipponi, S. Walther, P. Köhler, C. Frankenberg, L. Guanter, and A. Cescatti. 2020. "A Spatially Downscaled Sun-Induced Fluorescence Global Product for Enhanced Monitoring of Vegetation Productivity." *Earth System Science Data* 12 (2): 1101–1116. https://doi.org/10.5194/essd-12-1101-2020.

ESA. 2015. Report for Mission Selection: FLEX. Noordwijk, The Netherlands: ESA.

Fahad, S., A. A. Bajwa, U. Nazir, S. A. Anjum, A. Farooq, A. Zohaib, S. Sadia, et al. 2017. "Crop Production Under Drought and Heat Stress: Plant Responses and Management Options." *Frontiers in Plant Science* 8. https://doi.org/10.3389/fpls.2017.01147.

Farella, M. M., J. B. Fisher, W. Jiao, K. B. Key, and M. L. Barnes. 2022. "Thermal Remote Sensing for Plant Ecology from Leaf to Globe." *Journal of Ecology* 110 (9): 1996–2014. https://doi.org/10.1111/1365-2745.13957.

Farquhar, G. D., and T. D. Sharkey. 1982. "Stomatal Conductance and Photosynthesis." *Annual Review of Plant Physiology* 33 (1): 317–345. https://doi.org/10.1146/annurev.pp.33.060182.001533.

Féret, J.-B., K. Berger, F. de Boissieu, and Z. Malenovský. 2021. "PROSPECT-PRO for Estimating Content of Nitrogen-Containing Leaf Proteins and Other Carbon-Based Constituents." *Remote Sensing of Environment* 252:112173. https://doi.org/10.1016/j.rse.2020.112173.

Féret, J. B., A. A. Gitelson, S. D. Noble, and S. Jacquemoud. 2017. "PROSPECT-D: Towards Modeling Leaf Optical Properties Through a Complete Lifecycle." *Remote Sensing of Environment* 193:204–215. https://doi.org/10.1016/j.rse.2017.03.004.

Gates, D. M. 1968. "Transpiration and Leaf Temperature." *Annual Review of Plant Physiology* 19 (1): 211–238. https://doi.org/10.1146/annurev.pp.19.060168.001235.

Guzinski, R., H. Nieto, I. Sandholt, and G. Karamitilios. 2020. "Modelling High-Resolution Actual Evapotranspiration Through Sentinel-2 and Sentinel-3 Data Fusion." *Remote Sensing* 12 (9): 1433.

Hanuš, J., T. Fabiánek, and L. Fajmon. 2016. "POTENTIAL of AIRBORNE IMAGING SPECTROSCOPY at CZECHGLOBE." *International Archives of the Photogrammetry, Remote Sensing and Spatial Information Sciences* XLI-B1:15–17. archives-XLI-B1-15-2016",1,0,0>https://doi.org/10.5194/isprs-archives-XLI-B1-15-2016.

Hao, D., Y. Zeng, Z. Zhang, Y. Zhang, H. Qiu, K. Biriukova, M. Celesti, et al. 2022. "Adjusting Solar-Induced Fluorescence to Nadir-Viewing Provides a Better Proxy for GPP." *ISPRS Journal of Photogrammetry & Remote Sensing* 186:157–169. https://doi.org/10.1016/j.isprsjprs.2022.01.016.

Haxeltine, A., and I. C. Prentice. 1996. "A General Model for the Light-Use Efficiency of Primary Production." *Functional Ecology* 10 (5): 551–561. https://doi.org/10.2307/2390165.

Herrmann, I., and K. Berger. 2021. "Remote and Proximal Assessment of Plant Traits." *Remote Sensing* 13 (10). https://doi.org/10.3390/rs13101893.

IPCC. 2023. "Sections. In: Climate Change 2023: Synthesis Report. Contribution of Working Groups I, II and III to the Sixth Assessment Report of the Intergovernmental Panel on Climate Change." In edited by H. Lee and J. Romero, 35–115 . Geneva, Switzerland: IPCC. https://doi.org/10.59327/IPCC/AR6-9789291691647.

Lechner, A. M., G. M. Foody, and D. S. Boyd. 2020. "Applications in Remote Sensing to Forest Ecology and Management." *One Earth* 2 (5): 405–412. https://doi.org/10.1016/j.oneear.2020.05.001.

Liu, Z., F. Zhao, X. Liu, Q. Yu, Y. Wang, X. Peng, H. Cai, and X. Lu. 2022. "Direct Estimation of Photosynthetic CO2 Assimilation from Solar-Induced Chlorophyll Fluorescence SIF." *Remote Sensing of Environment* 271:112893. https://doi.org/10.1016/j.rse.2022.112893.

Ma, X., M. Migliavacca, J. F. B. Christian Wirth, A. Huth, R. Richter, and D. Miguel Mahecha. 2020. "Monitoring Plant Functional Diversity Using the Reflectance and Echo from Space." *Remote Sensing* 12 (8). https://doi.org/10.3390/rs12081248.

Malenovský, Z., L. Homolová, P. Lukeš, H. Buddenbaum, J. Verrelst, L. Alonso, M. E. Schaepman, N. Lauret, and J.-P. Gastellu-Etchegorry. 2019. "Variability and Uncertainty Challenges in Scaling Imaging Spectroscopy Retrievals and Validations from Leaves Up to Vegetation Canopies." *Surveys in Geophysics* 40 (3): 631–656. https://doi.org/10.1007/s10712-019-09534-y.

Moncholi-Estornell, A., M. Pilar Cendrero-Mateo, M. Antala, S. Cogliati, J. Moreno, and S. Van Wittenberghe. 2023. "Enhancing Solar-Induced Fluorescence Interpretation: Quantifying Fractional Sunlit Vegetation Cover Using Linear Spectral Unmixing." *Remote Sensing* 15 (17): 4274.

Moran, M. S., T. R. Clarke, Y. Inoue, and A. Vidal. 1994. "Estimating Crop Water Deficit Using the Relation Between Surface-Air Temperature and Spectral Vegetation Index." *Remote Sensing of Environment* 49 (3): 246–263. (94)90020-5",1,0,0>https://doi.org/10.1016/0034-4257(94)90020-5.

Moreno-Martínez, Á., G. Camps-Valls, J. Kattge, N. Robinson, M. Reichstein, P. van Bodegom, K. Kramer, et al. 2018. "A Methodology to Derive Global Maps of Leaf Traits Using Remote Sensing and Climate Data." *Remote Sensing of Environment* 218:69–88. https://doi.org/10.1016/j.rse.2018.09.006.

Nemani, R. R., C. D. Keeling, H. Hashimoto, W. M. Jolly, S. C. Piper, C. J. Tucker, R. B. Myneni, and S. W. Running. 2003. "Climate-Driven Increases in Global Terrestrial Net Primary Production from 1982 to 1999." *Science* 300 (5625): 1560–1563. https://doi.org/10.1126/science.1082750.

Pacheco-Labrador, J., M. P. Cendrero-Mateo, S. van Wittenberghe, G. Koren, and Z. Malenovský. 2022a. "Spatial Scaling Challenge - Additional Data. COST Action CA17134 SENSECO. Working Group 1." Zenodo. https://doi.org/10.5281/zenodo.6530187.

Pacheco-Labrador, J., M. P. Cendrero-Mateo, S. van Wittenberghe, G. Koren, and Z. Malenovský. 2022b. "Spatial Scaling Challenge. COST Action CA17134 SENSECO. Working Group 1." Zenodo. https://doi.org/10.5281/zenodo.6451335.

Pacheco-Labrador, J., M. Migliavacca, X. Ma, M. D. Mahecha, N. Carvalhais, U. Weber, R. Benavides, et al. 2022. "Challenging the Link Between Functional and Spectral Diversity with Radiative Transfer Modeling and Data." *Remote Sensing of Environment* 280:113170. https://doi.org/10.1016/j.rse.2022.113170.

Pacheco-Labrador, J., O. Perez-Priego, T. S. El-Madany, T. Julitta, M. Rossini, J. Guan, G. Moreno, et al. 2019. "Multiple-Constraint Inversion of SCOPE. Evaluating the Potential of GPP and SIF for the Retrieval of Plant Functional Traits." *Remote Sensing of Environment* 234:111362. https://doi.org/10.1016/j.rse.2019.111362.

Porwal, A., and A. E. Raftery. 2022. "Comparing Methods for Statistical Inference with Model Uncertainty." *Proceedings of the National Academy of Sciences* 119 (16): e2120737119. https://doi.org/10.1073/pnas.2120737119.

Poulter, B., N. MacBean, A. Hartley, I. Khlystova, O. Arino, R. Betts, S. Bontemps, et al. 2015. "Plant Functional Type Classification for Earth System Models: Results from the European Space Agency's Land Cover Climate Change Initiative." *Geoscientific Model Development* 8 (7): 2315–2328. 2315-2015",1,0,0>https://doi.org/10.5194/gmd-8-2315-2015.

Rocchini, D., and J. Lenoir. 2021. "Remote Sensing at the Interface Between Ecology and Climate Sciences." *Meteorological Applications* 28 (5): e2022. https://doi.org/10.1002/met.2022.

Ru, C., X. Hu, D. Chen, W. Wang, and J. Zhen. 2023. "Photosynthetic, Antioxidant Activities, and Osmoregulatory Responses in Winter Wheat Differ During the Stress and Recovery Periods Under Heat, Drought, and Combined Stress." *Plant Science* 327:111557. https://doi.org/10.1016/j.plantsci.2022.111557.

Running, S. W., R. R. Nemani, F. Ann Heinsch, M. Zhao, M. Reeves, and H. Hashimoto. 2004. "A Continuous Satellite-Derived Measure of Global Terrestrial Primary Production." *BioScience* 54 (6): 547–560. (2004)054[0547:ACSMOG]2.0.CO;2",1,0,0>https://doi.org/10.1641/0006-3568(2004)054[0547:ACSMOG]2.0.CO;2.

Schimel, D., F. D. Schneider, J. P. L. Carbon, and E. Participants. 2019. "Flux Towers in the Sky: Global Ecology from Space." *New Phytologist* 224 (2): 570–584. https://doi.org/10.1111/nph.15934.

Siegmann, B., L. Alonso, M. Celesti, S. Cogliati, R. Colombo, A. Damm, S. Douglas, et al. 2019. "The High-Performance Airborne Imaging Spectrometer HyPlant—From Raw Images to Top-Of-Canopy Reflectance and Fluorescence Products: Introduction of an Automatized Processing Chain." *Remote Sensing* 11 (23). https://doi.org/10.3390/rs11232760.

Song, Z., L. Wang, M. Lee, and G. Hua Yue. 2023. "The Evolution and Expression of Stomatal Regulators in C3 and C4 Crops: Implications on the Divergent Drought Tolerance." *Frontiers in Plant Science* 14. https://doi.org/10.3389/fpls.2023.1100838.

van der Tol, C., W. Verhoef, J. Timmermans, A. Verhoef, and Z. Su. 2009. "An Integrated Model of Soil-Canopy Spectral Radiances, Photosynthesis, Fluorescence, Temperature and Energy Balance." *Biogeosciences* 6 (12): 3109–3129. 3109-2009",1,0,0>https://doi.org/10.5194/bg-6-3109-2009.

Van Wittenberghe, S., N. Sabater, M. P. Cendrero-Mateo, C. Tenjo, A. Moncholi, L. Alonso, and J. Moreno. 2021. "Towards the Quantitative and Physically-Based Interpretation of Solar-Induced Vegetation Fluorescence Retrieved from Global Imaging." *Photosynthetica* 59 (3): 438–457. https://doi.org/10.32615/ps.2021.034.

Verhoef, W. 1984. "Light Scattering by Leaf Layers with Application to Canopy Reflectance Modeling: The SAIL Model." *Remote Sensing of Environment* 16 (2): 125–141. (84)90057-9",1,0,0>https://doi.org/10.1016/0034-4257(84)90057-9.

Verhoef, W., C. van der Tol, and E. M. Middleton. 2018. "Hyperspectral Radiative Transfer Modeling to Explore the Combined Retrieval of Biophysical Parameters and Canopy Fluorescence from FLEX – Sentinel-3 Tandem Mission Multi-Sensor Data." *Remote Sensing of Environment* 204:942–963. https://doi.org/10.1016/j.rse.2017.08.006.

Verrelst, J., G. Camps-Valls, J. Muñoz-Marí, J. Pablo Rivera, F. Veroustraete, J. G. P. W. Clevers, and J. Moreno. 2015. "Optical Remote Sensing and the Retrieval of Terrestrial Vegetation Bio-Geophysical Properties – a Review." *ISPRS Journal of Photogrammetry & Remote Sensing* 108:273–290. https://doi.org/10.1016/j.isprsjprs.2015.05.005.

Verrelst, J., Z. Malenovský, C. Van der Tol, G. Camps-Valls, J.-P. Gastellu-Etchegorry, P. Lewis, P. North, and J. Moreno. 2019. "Quantifying Vegetation Biophysical Variables from Imaging Spectroscopy Data: A Review on Retrieval Methods." *Surveys in Geophysics* 40 (3): 589–629. https://doi.org/10.1007/s10712-018-9478-y.

Vicente, B.-L., H. Nieto, D. Riaño, M. Migliavacca, T. S. El-Madany, R. Guzinski, A. Carrara, and M. Pilar Martín. 2021. "The Effect of Pixel Heterogeneity for Remote Sensing Based Retrievals of Evapotranspiration in a Semi-Arid Tree-Grass Ecosystem." *Remote Sensing of Environment* 260:112440. https://doi.org/10.1016/j.rse.2021.112440.

Vivone, G. 2023. "Multispectral and Hyperspectral Image Fusion in Remote Sensing: A Survey." *Information Fusion* 89:405–417. https://doi.org/10.1016/j.inffus.2022.08.032.

Wang, S., K. Guan, Z. Wang, E. A. Ainsworth, T. Zheng, P. A. Townsend, K. Li, C. Moller, G. Wu, and C. Jiang. 2021. "Unique Contributions of Chlorophyll and Nitrogen to Predict Crop Photosynthetic Capacity from Leaf Spectroscopy." *Journal of Experimental Botany* 72 (2): 341–354. https://doi.org/10.1093/jxb/eraa432.

Wang, S., K. Guan, Z. Wang, E. A. Ainsworth, T. Zheng, P. A. Townsend, N. Liu, et al. 2021. "Airborne Hyperspectral Imaging of Nitrogen Deficiency on Crop Traits and Yield of Maize by Machine Learning and Radiative Transfer Modeling." *International Journal of Applied Earth Observation and Geoinformation* 105:102617. https://doi.org/10.1016/j.jag.2021.102617.

Weiss, M., F. Jacob, and G. Duveiller. 2020. "Remote Sensing for Agricultural Applications: A Meta-Review." *Remote Sensing of Environment* 236:111402. https://doi.org/10.1016/j.rse.2019.111402.

Widlowski, J.-L., C. Mio, M. Disney, J. Adams, I. Andredakis, C. Atzberger, J. Brennan, et al. 2015. "The Fourth Phase of the Radiative Transfer Model Intercomparison (RAMI) Exercise: Actual Canopy Scenarios and Conformity Testing." *Remote Sensing of Environment* 169:418–437. https://doi.org/10.1016/j.rse.2015.08.016.

Wieneke, S., J. Pacheco-Labrador, M. D. Mahecha, S. Poblador, S. Vicca, and I. A. Janssens. 2024. "Comparing the Quantum Use Efficiency of Red and Far-Red Sun-Induced Fluorescence at Leaf and Canopy Under Heat-Drought Stress." *Remote Sensing of Environment* 311:114294. https://doi.org/10.1016/j.rse.2024.114294.

Yang, J., P. Gong, R. Fu, M. Zhang, J. Chen, S. Liang, B. Xu, J. Shi, and R. Dickinson. 2013. "The Role of Satellite Remote Sensing in Climate Change Studies." *Nature Climate Change* 3 (10): 875–883. https://doi.org/10.1038/nclimate1908.

Yang, P., E. Prikaziuk, W. Verhoef, and C. van der Tol. 2021. "SCOPE 2.0: A Model to Simulate Vegetated Land Surface Fluxes and Satellite Signals." *Geoscientific Model Development* 14 (7): 4697–4712. https://doi.org/10.5194/gmd-14-4697-2021.

Zandalinas, S. I., R. Mittler, D. Balfagón, V. Arbona, and A. Gómez-Cadenas. 2018. "Plant Adaptations to the Combination of Drought and High Temperatures." *Physiologia plantarum* 162 (1): 2–12. https://doi.org/10.1111/ppl.12540.